 CMES, vol.6, no.5, pp.409-420, 2004

Geometry of Flow Pattern from Single Source

C. K. Au[1]

Abstract: Tracking the flow fronts arising from a primary source in a bounded space with obstacles is a problem which often requires intensive computation. As the flow propagates through the obstacles, the flow pattern is complicated. This phenomenon is mainly due to the existence of the secondary sources which can be identified in the flow field by visibility. Comparing the flow fronts propagation and the wave equation reveals that the complexity is caused by the propagation phenomena: reflection, refraction, diffraction and interference. This paper investigates a geometric technique to combine these phenomena for computing flow fronts.

keyword: flow fronts, reflection, refraction, diffraction, interference

1 Overview

One of the earliest methods for constructing the progression of wave fronts is due to Huygens. Each point on a wave front is considered as a secondary source that propagates in radial direction with due regards to directionally dependent velocities – the envelope of which forms the wave front for the next instance in time. Geometrically, it is recalled fondly the notion of a "variable radius offset". The offset radii differ not only at different point on a curve but also in different directions, giving the effect of an anisotropic medium with tensor properties. In the presence of abrupt discontinuity such as a blunt obstacle, phase must also be taken into account in the superposition of amplitudes. This latter consideration of phase owes to Fresnel in his study of diffraction.

An obstacle in a flow stream presents two apertures, through which the material flows around it. Beyond the obstacle, the two branches of the flow meet and interact. Depending on the velocity and material coefficients, there can be vortices and chaos. Intellectually, at the *wave* or phenomenological level (whereby flow of material is modeled as partial differential equations), a lot has already been done in the last one hundred years. Indeed, thanks to inexpensive computing power, solutions to fluid flow problems are abundantly available by the various modeling techniques such as the finite element method and numerical integration schemes. Yet, at the *particulate* level (where atoms or molecules interact), there is a large amount of current activities. Perhaps stimulated the promise in biotechnology and nanotechnology, biologists, chemists, material scientists and physicists are studying "molecular dynamics" with vigor. It may be prudent to ask what the intellectual obstacle, that might challenge most researchers, would be. The answer appears simple, though the mean is not: the curse of combinatorial explosion. Manifested in the form of the "Many Body Problem", such a challenge has been recognized by many distinguished scientists, from Newton's time to the present day. (It may be interesting to know that the Feynman diagram, for analyzing the Many Body Problem, involves series expansion – with each term being a set of wave equations demanding their own solutions.) It appears that the challenge remains daunting at the particulate level.

By combining the wave and the particulate approaches, this paper offers a fast *geometric* approximation to flow propagation. Figure 1 illustrates the geometric solution, as compared to the numerical solution (from a commercially available package for simulating mould flow by finite element method). A source emitting flow is located at the lower left corner of a maze. The flow propagates through the partitions of the maze which act as the obstacles. It may be noted that the spacing between the successive flow fronts in the geometric solution is uniform. This is because of the simplicity in the geometry adopted by this paper.

2 Source

For each source $\mathbf{j}$, define a space time function $\phi(r,t)$ for an arbitrary point $\mathbf{p}$ in a domain $\mathbf{D}(=\mathbf{R}^2)$ as a mapping ϕ:

[1] School of Mechanical Engineering, Nanyang Technological University, Singapore, 639798 mckau@ntu.edu.sg

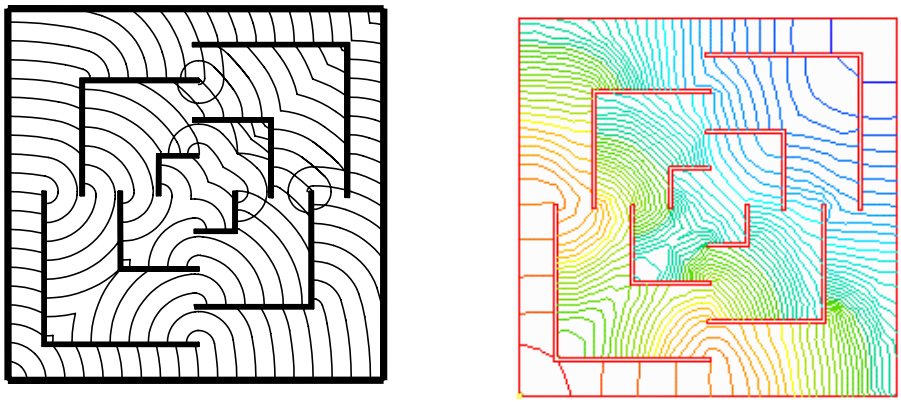

(a) geometric solution (b) numerical solution

Figure 1 : The geometric and numerical solution of the flow in a maze

$\mathbf{R}\times\mathbf{R}\rightarrow\mathbf{R}$ such that:

$$\phi(r,t) = \quad (t_j - t) + \frac{r}{v_j} \tag{1}$$

where t_j and v_j are the characteristics of the source **j** that are non-negative constants; and r is the distance from any point **p** to the source **j**.

Space time function (1) satisfies the flow front $\mathbf{\Gamma}$ equation from a point source is derived from the conservation law

$$\frac{\partial\phi}{\partial t} + \frac{\partial(v_j \cdot \phi)}{\partial r} = 0 \tag{2}$$

where v_j is the velocity of the flow and;

r is the distance between the source and the flow front.

The flow front $\mathbf{\Gamma}$ is defined as $\mathbf{\Gamma}(t) = \{r|\phi(r,t) = 0\}$. For a point source **j**, the initial front is given as $\mathbf{\Gamma}(0) = \{r|\phi(0,t_j) = 0\}$ and the source starts emitting at time t_j. Equation (2) is a kinematic description of the propagation of the front in the direction perpendicular to itself. The flow front $\mathbf{\Gamma}(t) = \{r|\phi(r,t) = 0\}$ suggests that both space (in term of r) and time (in term of t) are needed to consider in the tracking process.

Differentiating equation (2) with respect to time t and space r with the assumption of constant velocity v_j yields the equation

$$\frac{\partial^2\phi}{\partial t^2} = v_j^2 \frac{\partial^2\phi}{\partial r^2} \tag{3}$$

The similarity between equation (3) and the planar wave equation reveals that wave propagation phenomena such as reflection, refraction, diffraction and interference are expected in the flow.

A source **j** in a two-dimensional free space without boundaries is characterized by two parameters: the propagation velocity v_j and the time of emission t_j. For isotropic medium with constant refractive index, the circular flow fronts are emitted spatially. Temporally, the radius of the circular flow fronts increase with time. The space time function of such a source can be represented by an inverted cone with a "stem" as shown in figure 2(a). The propagation velocity v_j is the arctangent of the cone angle. The stem is the geometric representation of the delay in emission. In the case of medium with variable refractive index, the space time geodesic will no longer be a straight line and the cone will be distorted. For instance, a medium with refractive index as linear function of the y coordinate from the source gives a catenary as the geodesic. The distorted cone in space time is shown in figure 2(b). The metric of such a space is no longer Euclidean.

Consider the propagation in a two dimensional Euclidean space with a primary source. The emission delay is zero. The other $(N \quad -1)$ secondary sources arise owing to the obstacles in the space, hence manifesting a time delay in their engagement. Hence, the space time function for all these N sources (both primary and secondary) are represented by a set of N inverted cones with various stems. The delay for a secondary source is the time for the propagation from one source to another. The resultant space time function of the propagation is represented by a composite cone which is the Boolean sum of all the inverted

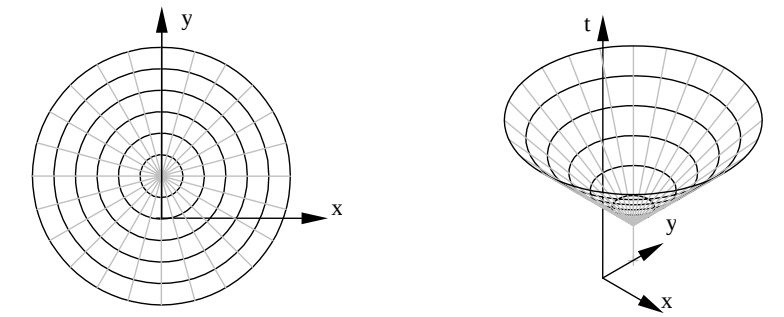

the geodesics and flow fronts — the space time function

(a) source **j** with constant emission velocity v_j, engaging at time $t = t_j$

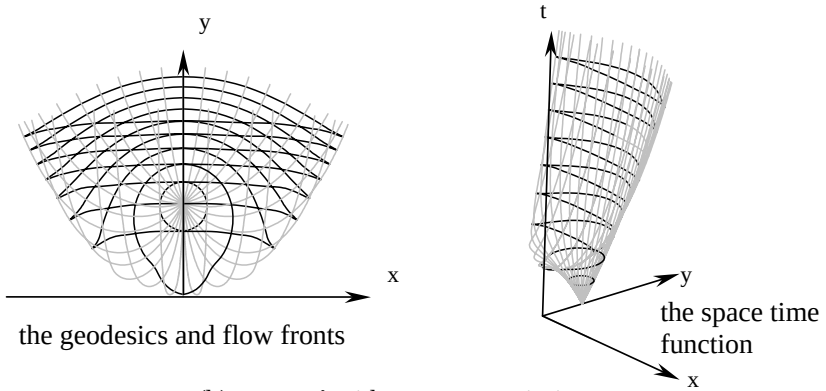

the geodesics and flow fronts

(b) source **j** with constant emission velocity $v_j = \frac{k}{y}$, engaging at time $t = 0$

Figure 2 : Model of a source

cones. The calculation for the geometric approximation of the flow fronts becomes a simple matter of taking horizontal time slices of a composite cone.

To construct the composite cone, techniques for identifying a secondary source (as the apex of a cone with a time delay) are borrowed from geometrical optics, with the aid of figure 3.

Reflection occurs in the flow from a primary source in a bounded domain; see figure 3(a). Trivially, the virtual source is located at equal distance but on the other side of a reflector.

Refraction arises in the flow through an interface between two media; see figure 3(b). The location of a virtual source is not entirely obvious.

Diffraction appears in the flow from a small area to a large area. Figure 3(c) shows how the flow front turns around the corners as it propagates from a small channel to a larger channel.

Interference happens in the flow behind an obstacle. Figure 3(d) shows a triangular obstacle in the flow stream. In fluids, this is a two-channel flow; from optics, there are two apertures. Waves emerging through them will interfere while a "weld line" will be created in material flow.

Flow front generation arises in many areas such as biology, logistics and manufacturing. The most vivid example from manufacturing would be the mould and die filling. Tracking the flow fronts is important since the flow pattern affects the quality of the part. Front tracking methods [Defermos (1972), Holden, Holden, and Hoegh-Krohn (1988)] are based on a Lagrangian

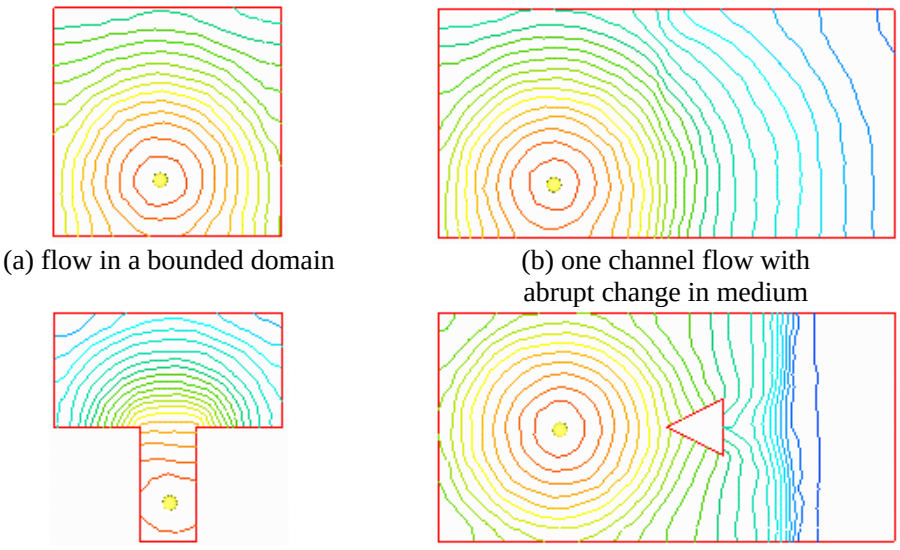

(a) flow in a bounded domain

(b) one channel flow with abrupt change in medium

(c) flow, one channel, with abrupt change in geometry

(d) two channels flow

Figure 3 : Melt flows in various situations

formulation. Numerical instability is the major issue of these methods. Grid based methods such as narrow band method [Sethian (1999)] and fast marching method [Chopp (1993)] are two common approaches to solve the partial differential equations. Level set method [Sethian (1996)] avoids such complex problem by using a level set function which is given an Eulerian co-ordinate system to represent the moving fronts. Besides flow front tracking, level set method is widely used in various applications such as geometric optics [Cheng, Kang, Osher, Shim, and Tsai (2004)], heterogeneous material modelling [Sheen, Seo, and Cho (2003)] etc.

Meshing is the fundamental to both grid based methods and finite element method to solve for the flow problem. Finite elements are accurate enough to solve for the two and, two and half dimensional flow front advancement problem. Medial axis and surface [Quadros, Ramaswami, Prinz, Gurumoorthy (2000)] are the techniques to extract the mid-plane of a three dimensional geometric model. Two dimensional mesh is generated on the mid-plane model.

3 Visibility

The flow path is the propagation route in the flow field. Under the principle of least action, these flow paths are the geodesic curves, which are equivalent to the lines of sight, from the source. Under the assumption of no external forces acting in the flow field, the line of sight would be a straight line. The partition of the flow field covered by the flow from a source is the region which is totally visible by the source. As a result, the line of sight can be constructed from any point in the partition to the source.

Huygen's principle describes the local propagating pattern from a source **j** by considering each point on the flow front as a point source. Hence, each point on the rim of the inverted cone is a source. The envelope that contains all the local propagating patterns constitutes the new flow front. Visibility from a point source is employed to identify the secondary source. For a given polygon, the lines of sight are generated from the source in various directions. Secondary source arises when any of the lines of sight hits a reentrant vertex. In the figure 4, $\mathbf{abk_1k_2cdefgh}$ is a bounded polygon of flow field. **j** is the primary source. $\mathbf{jk_1}$ is the line of sight from **j**. The partition $\mathbf{abk_1gh}$ is covered by the primary source **j**, hence every point in this partition is visible to the source **j**. A secondary source $\mathbf{k_1}$ is identified when the line of sight from **j** hits the vertices of the polygon since $\mathbf{k_1}$ is the only point source on the flow front that enters the partition $\mathbf{k_1k_2cdefg}$. Due to the existence of another reentrant vertex $\mathbf{k_2}$, the partition is further sub-divided into two sub-partitions: $\mathbf{k_1k_2efg}$ and $\mathbf{k_2cde}$. Every point in the partitions $\mathbf{k_1k_2efg}$ and $\mathbf{k_2cde}$ is visible to the secondary

source $\mathbf{k}_1$ and $\mathbf{k}_2$ respectively.If t_j and v are the source characteristics of **j**, then source characteristics for secondary sources $\mathbf{k}_1$ and $\mathbf{k}_2$ are $t_{k_1} = t_j + \frac{d_{jk_1}}{v}$ (where d_{jk_1} is the distance between **j** and $\mathbf{k}_1$) and $v_{k_1} = v$ (constant filling velocity is assumed) and; $t_{k_{21}} = t_j + \frac{d_{jk_1}}{v} + \frac{d_{jk_2}}{v}$ and $v_{k_2} = v$ respectively.

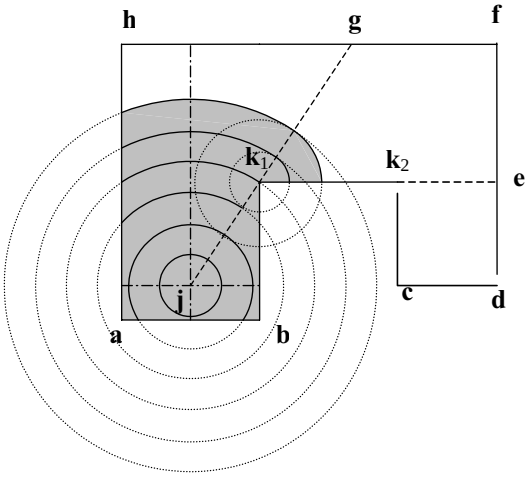

Figure 4 : Secondary source identification by visibility

4 Voronoi diagram

Besides the geometry of the polygon and the obstacle, the geometry of the flow front in two dimensional Euclidean domain depends upon the geometry of the source. For instance, linear flow fronts will be generated from a line source in a medium with constant index of refraction while a point source gives the circular flow fronts. The complexity of the flow increases with the number of sources. The arising of multiple sources would be due to either the multiple primary sources such as the multiple-gate cavity in injection moulding or the obstacles in the flow field. As the flow propagates around the obstacles, secondary sources exist. The flow field is partitioned into several regions in these cases, one for each source (either primary or secondary) to fill up. Hence, a Voronoi diagram exists in the flow field partitioning. The frontier between the Voronoi cells, termed as Voronoi curve, is where the flow fronts meet. The weld line in the plastic injection moulding is the flow phenomenon due to the Voronoi cells. The partitioning of the three-gate cavity in figure 5 is a typical example of the Voronoi diagram in computational geometry.

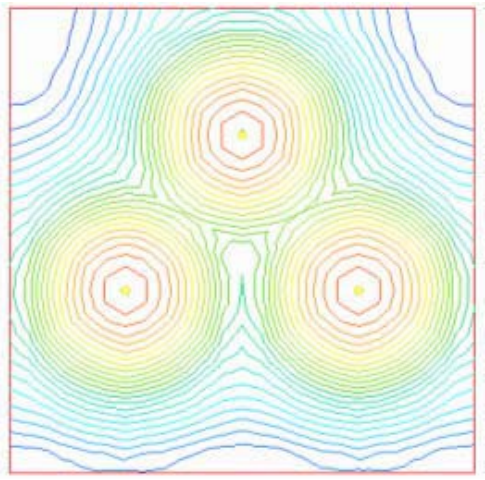

Figure 5 : Voronoi diagram of a multi-gate cavity

For each source **j**, either a gate or a secondary source induced by the obstacles; possesses two source characteristics: v_j and t_j. The geometry of the Voronoi curve between two partitions covered by two sources **j** and **k** is defined by the ratio of these two characteristics [Au and Woo (2004)]: $\alpha = \frac{v_k}{v_j}$ and $\beta = \frac{t_k}{t_j}$. More detail discussions on Voronoi diagrams can be found in [Okabe, Boots, Sugihara, and Chiu (2000)]. Yet there is a deeper and more beautiful structure in the equilibrium between two sources, owing to the parametrization of the quartic polynomial by α and β [Au and Woo (2004)].

5 Flow front propagation

An undistorted space time function for a point source **j** is an inverted cone. The flow paths from **j** to a specific point in the flow field are the projection of the geodesics from the apex of the cone to corresponding points on the space time function on to the space. Hence, if constant flow velocity is assumed, the flow paths from a point source **j** are in radial direction perpendicular to the fronts. The phenomena of reflection, refraction, diffraction and interference are due to the distortion of the space time function which causes changes in the flow.

5.1 Reflection

The space time function of a source **j** emitting at t_j with velocity v_j in Euclidean domain is an inverted cone and is considered as flat since its Gaussian radius is zero.

The reflected path in the flow field is governed by the law

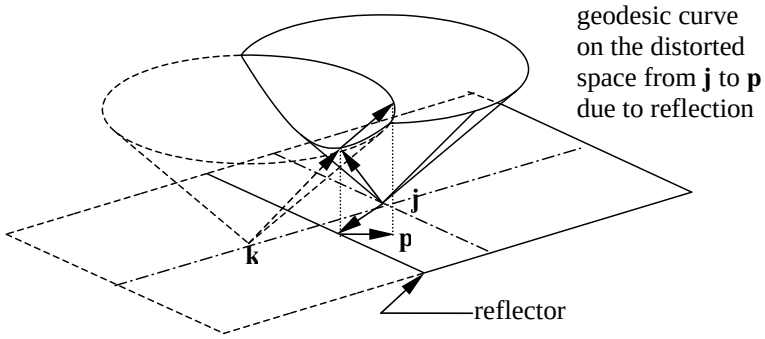

(a) the space time function of a source due to reflection

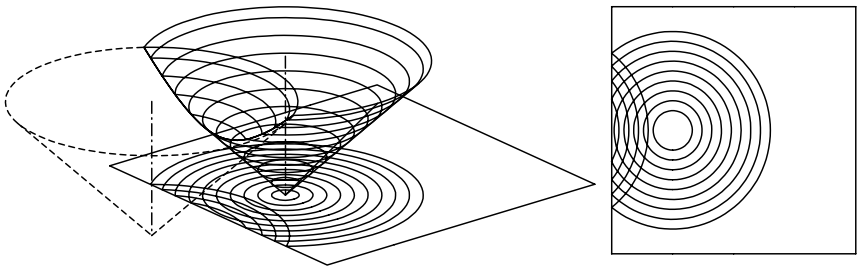

(b) sectioning of the space time function (c) flow front

Figure 6 : The flow front due to reflection

of reflection

$$\frac{\sin\theta_1}{\sin\theta_2} = -1 \tag{4}$$

where θ_1 and θ_2 are the angle of incidence and reflection. The negative sign indicates the reverse path due to reflection.

The existence of the boundary (act as a reflector) produces a virtual source **k**. This virtual source produces another virtual inverted cone which distorts the space time function as shown in figure 6(a). Since $\alpha = \left|\frac{v_k}{v_j}\right| = 1$ and $\beta = 1$(both sources emit at the same time). The reflector in this case is the Voronoi curve between two "sites": **j** and **k**. The path in the flow field from the source **j** to a point **p** through reflection is the space projection of geodesic curve from **j** to the point corresponding to **p** on the distorted space time. Figure 6(b) shows the sectioning of the space time function due to reflection and the flow fronts are obtained by the space projection as shown in figure 6(c).

Figure 7(a) shows a flow front with reflection suppressed. The flow front obtained by space projection is compared with the filling pattern produced by Moldflow[2] in figure 7(b). The Moldflow plot does not show the reflection probably due to the low Reynold's number. Hence, either the soft boundaries or boundary sink are assumed.

In this paper, the number of reflections is limited to zero. In other words, given a reflector, a primary source generates no virtual sources.

5.2 Refraction

The path of the flow due to refraction is determined by the Snell's law

$$\frac{\sin\theta_1}{\sin\theta_2} = \eta \tag{5}$$

where θ_1 and θ_2 are the angle of incidence and refraction and; η is the index of refraction.

Comparing equation (4) and (5) reveals that both reflection and refraction are topologically equivalent. Hence, the space time function should also be distorted due to

[2] Moldflow is a plastic flow analysis software based on finite element method from Moldflow Inc. (http://www.moldflow.com)

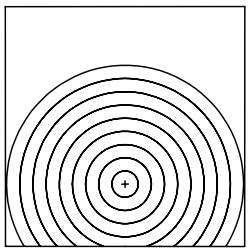

(a) flow front with reflection suppressed

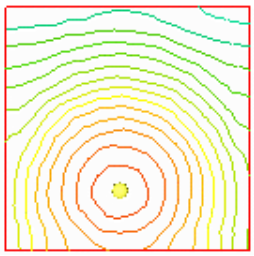

(b) Moldflow plot

Figure 7 : The flow fronts and the Moldflow plot

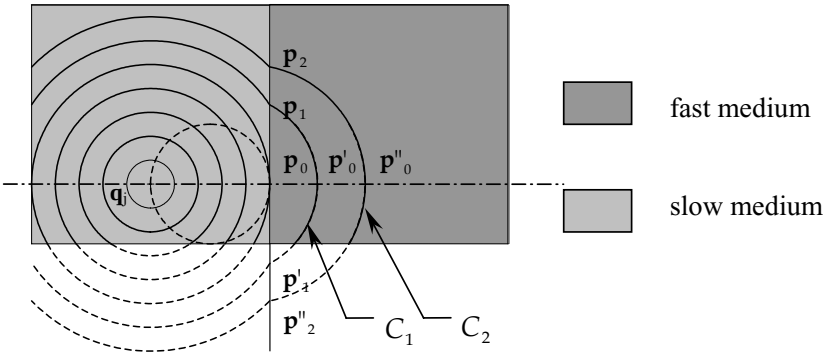

Figure 8 : Flow fronts in refractive environment

the refraction. Figure 8 illustrates the propagation of the flow front in refractive environment. This phenomenon in the flow is manly caused by the variation of flow velocity in different medium of the flow field.

At t_0, the flow front is at $\mathbf{p}_0$. After a time interval Δt, the flow front hits the interface at $\mathbf{p}_1$ and virtually $\mathbf{p}'_1$ while the flow front propagates from $\mathbf{p}_0$ to$\mathbf{p}'_0$. At $t_0 + 2\Delta t$, the flow front at $\mathbf{p}_1$,$\mathbf{p}'_1$ and $\mathbf{p}'_0$ moves to $\mathbf{p}_2$,$\mathbf{p}'_2$ and $\mathbf{p}$"$_0$. The flow fronts through the points $\mathbf{p}_1$,$\mathbf{p}'_1$, $\mathbf{p}'_0$ and $\mathbf{p}_2$,$\mathbf{p}'_2$,$\mathbf{p}$"$_0$ are approximated by two circular arcs C_1 and C_2. Obviously, these arcs are not concentric, but they are collinear with the source **j**.

Hence if the flow fronts in the fast moving medium are generated by a secondary source **k** due to refraction along the interface, then this source is a *moving* source [Au and Woo (2004)]. Figure 9 illustrates the relationship between the primary source **j** and secondary source **k**.

The space time function is distorted by the moving secondary source due to the change in propagation velocity as shown in figure 10(a). The α and β ratios for these two sources are $\frac{v_k}{v_j}$ and $\left|\left(t_j + \frac{d}{v_j}\right)\frac{1}{t_j}\right|$ respectively, where d is

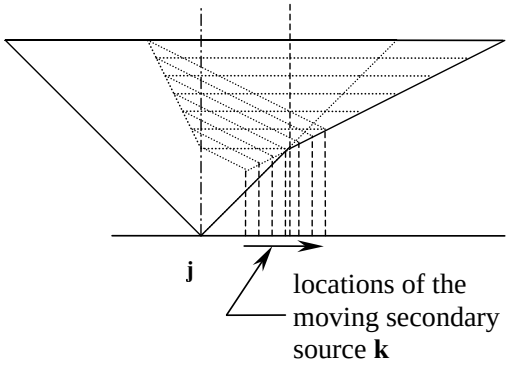

Figure 9 : The space time of the primary and the moving secondary source

the distance from the gate to the interface. The Voronoi curve in this case is a straight line because β for these sources is a constant (as d is not a constant). This is an example of a Voronoi diagram of one fixed and one moving site. Slicing the distorted function and projecting on to the space gives the flow fronts as depicted in figure

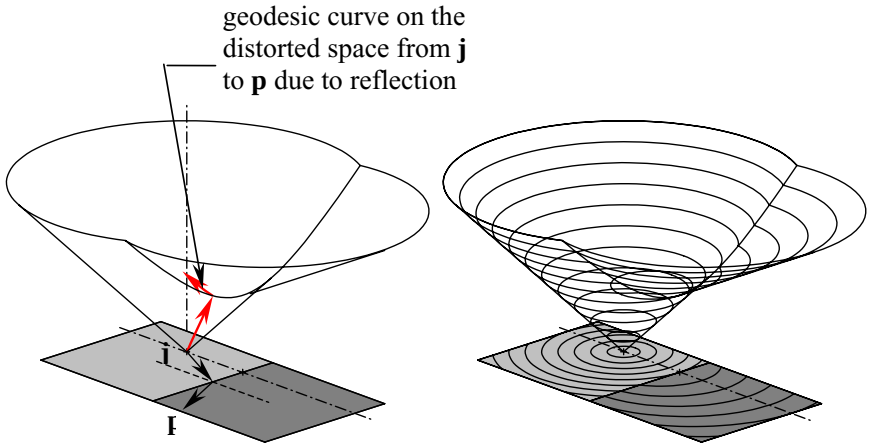

(a) the distorted space time function due to refraction

(b) sectioning of the space time function

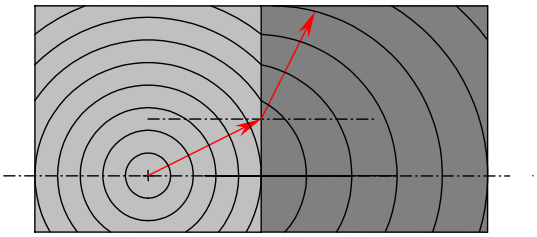

(c) flow front

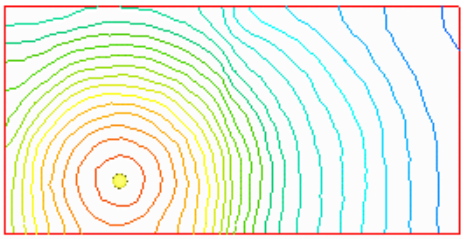

(d) filling pattern generated by Moldflow

Figure 10 : The flow front due to refraction

10(b). Figure 10(c) is the top view of the space. The flow fronts are compared to the filling pattern generated by Moldflow in figure 10(d).

5.3 Diffraction

The flow in the flow field will be deflected if there is an abrupt change in flow width such as widened as shown in figure 4(c). This also happens when the flow hits the obstacles. For example, the inserts in mould and die cavity are common obstacles in the flow since these inserts narrow the widths of the flow channel. Obviously, the flow deflection is caused by the distortion of the space time function due to the narrowness of the flow channel.

For an unbounded domain, the flow path will be a straight line which is a geodesic curve in the flat Euclidean space. This is analogous to the line of sight from the source (or gate).

If the domain is bounded and with the assumption that the boundary is absorbent offering no reflection, a secondary source arises at the point where the line of sight

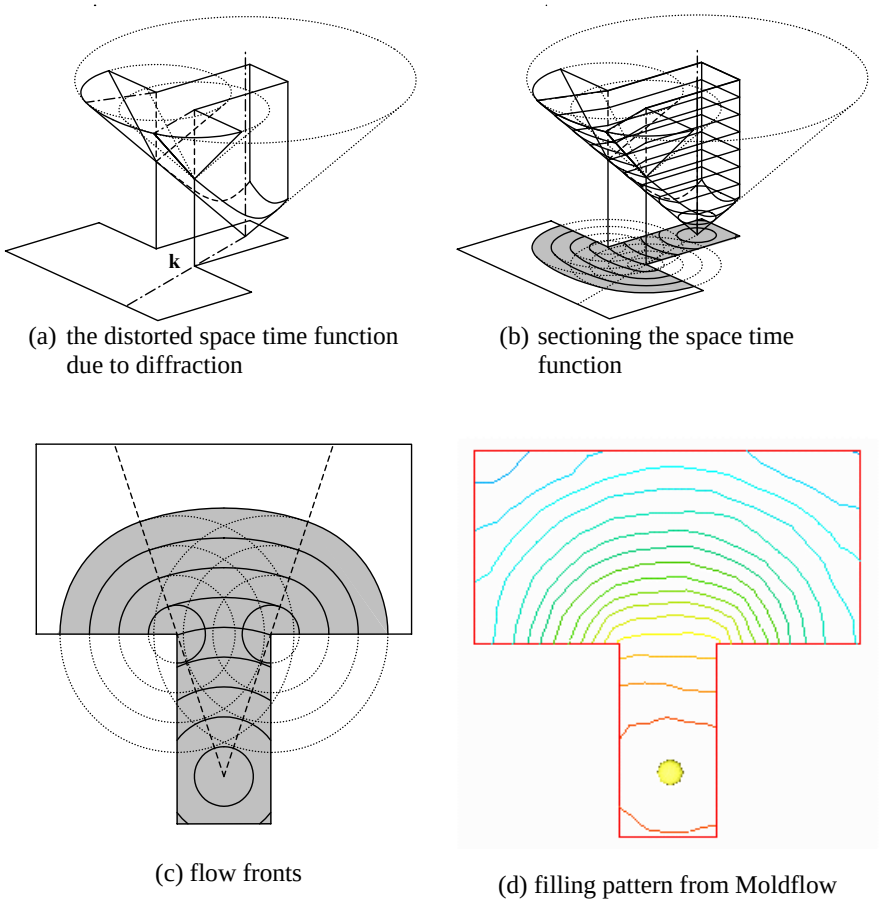

(a) the distorted space time function due to diffraction

(b) sectioning the space time function

(c) flow fronts

(d) filling pattern from Moldflow

Figure 11 : Flow front due to diffraction

hits the boundary (either the boundary of the polygon or the obstacles). In this case, the flow field is partitioned since there are more than one source, a primary and the secondary sources. The secondary source is not inhibited for the flow from the source and is stopped by the boundary and the Voronoi curve. The space time geometry of the source is trimmed off due to the boundary of the flow field and the line of sight.

The source characteristics for primary source **j** is v_j (assume constant flow velocity) and t_j(=0, zero time delay) while the characteristics for the secondary source **k** is v_j and $t_k \left(= \frac{d_{jk}}{v_j}\right)$, where d_{jk} is the geodesic distance between **j** and **k**. Figure 11(a) shows the space time function. The secondary source is flared out due to the line of sight **jk**.

The flow fronts are obtained by sectioning the distorted space time geometry as illustrated in figure 11(b) and projecting on to the (2D) space as shown in figure 11(c). A similar Moldflow plot is shown in figure 11(d).

5.4 Interference

Under certain circumstances, two virtual sources exist and cause interference (for wave propagation) or weld line (for plastic flow). The flow field is partitioned according to the line of sights from the sources. Interference arises when there is more than one source in the partition. In this case, a Voronoi curve is formed when two flow front meet each other. With $\alpha = 1$(constant flow velocity is assumed), the lines of sight are the Voronoi curves of the partitions.

The flow field is partitioned by the line of sight because of the obstacles. These bounded partitions distort the space time function. The distorted space time function due to the diffractions is shown in figure 12(a). The flow fronts are obtained by sectioning the distorted space time function and projecting on to the space as depicted in figure 12(b). The flow fronts are shown in figure 12(c). Fig-

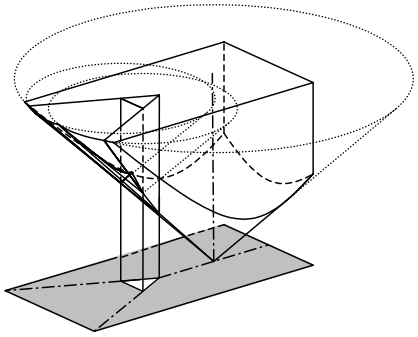

(a) distorted space time function

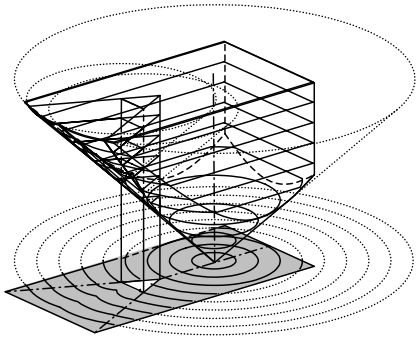

(b) flow fronts from the space time function

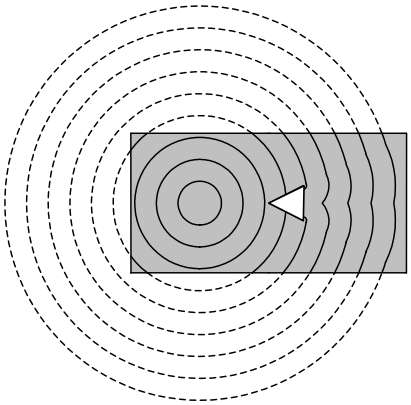

(c) flow front

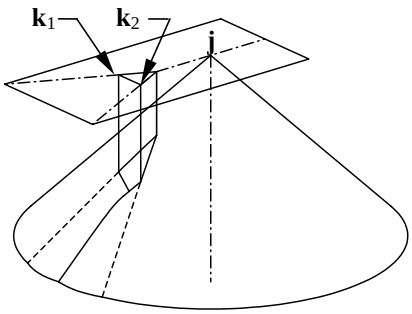

(d) bottom side of the space time function

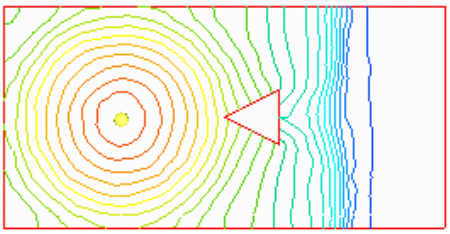

(e) Filling pattern from Moldflow

Figure 12 : Flow front due to diffractions and causes weld line

ure 12(d) shows the bottom view of the space time function (bottom view is used for easy visualization). The time delays for the two secondary sources $\mathbf{k}_1$ and $\mathbf{k}_2$ are also shown. The Modlflow plot is shown in figure 12(e) for comparison.

6 Example

The flow deflection is mainly caused by two features in the flow field: obstacle and change in flow velocity. When these features exist in the flow field, the space time function is distorted. The flow paths in the flow field are the projection of the geodesics on the space time function on to the space.

Figure 13(a) shows a flow field with two different media so that the flow velocity ratio in region j and region k is $\frac{v_j}{v_k} = \frac{1}{1.5}$. An obstacle is in the region k. Flow enters the filed from the source **j**. Refraction occurs at the interface between region j and region k, hence the lines of sight from the primary source **j** entering region k is not straight lines. Four secondary sources $\mathbf{k}_1$, $\mathbf{k}_2$, $\mathbf{k}_3$ and $\mathbf{k}_4$

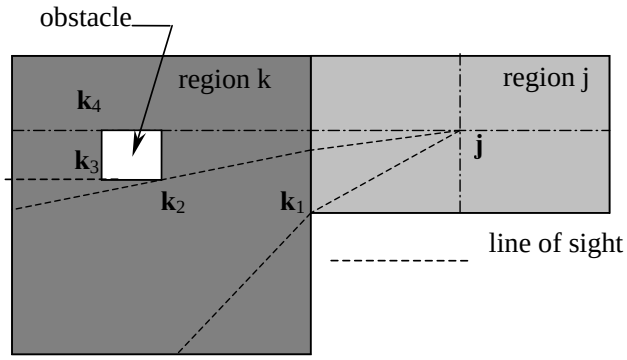

(a) cavity with secondary sources

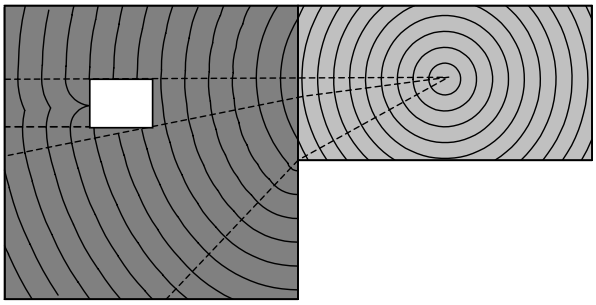

(b) flow pattern

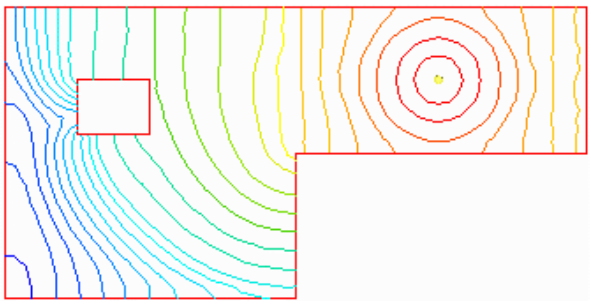

(c) Moldflow plot

Figure 13 : A cavity with different flow velocity

are identified. Each secondary source possesses different time delay and constant flow velocity in each region is assumed. The flow front due to the distorted space time is shown in figure 13(b).

Figure 14 shows the space time function at the instant just before the two dimensional domain being fully filled up. The time axis t of the function points downward for easy visualization. The time delays for various secondary sources are also shown in the figure. There is a discontinuity in the space time function which accounts for the existence of a Voronoi curve after the obstacle. Since the time delays for secondary sources $\mathbf{k}_3$ and $\mathbf{k}_4$ are different, the geometry of the Voronoi curve is a circular arc, not a straight line as discussed in reference [Au and Woo (2004)].

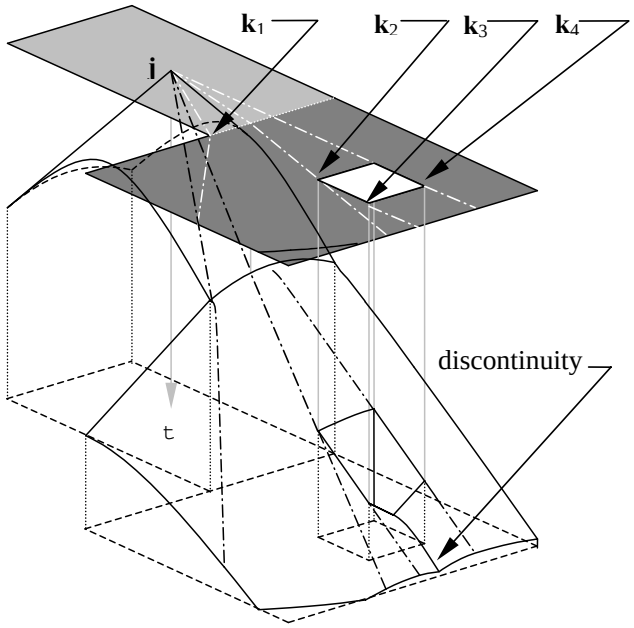

Figure 14 : The space time function of the flow field

7 Assumption revisited

Manufacturing operations such as moulding, casting, heat treatment, rolling, forming, and forging involve shape changes. Quantitative assessment and prediction of the result have always required the solution to partial differential equations from fluid dynamics and thermodynamics, the modeling of which require insight in the particular process under consideration. Then, too, the solution to the partial differential equations involving integration under boundary conditions is known to be difficult. Approximation techniques necessarily incur errors.

The study of waves can be daunting, while its history can be interesting. Typically, the work involves the modelling of appropriate partial differential equations and then solving them subject to the certain boundary conditions. In the context of kinetic geometry, the waves are the “moving fronts” or “evolving curves”. Yet, when position and derivatives changes, one may also inquire what remains invariant. The conservation of energy and

momentum necessarily follows. As well, when multiple paths for a change (or a variation) are possible, selection naturally arises. Two branches of science prominently anchor the geometric notion of waves and shortest path: optics and continuum mechanics. Underlying both is optimality.

This paper gives an approximate solution to wave phenomena arising in the flow field. It offers a fast analytical solution to a class of partial differential equation, known as the Hamilton-Jacobi equations in continuum mechanics or the Eikonal equations in geometrical optics. Because the computation involves no more than algebra, the performance is in real time. Yet, to be truly convincing, a Kirchoff-like reverse-engineering of the wave equations from the geometry is to be accomplished, monumental the task appears to be.

The velocity of flow is assumed to be constant. In fact it is governed by three major equations: continuity equation, momentum equation and energy equation. Representing the space time function of a source as an inverted cone implies the constant filling velocity when solving the flow front equation (2). This assumption simplifies the flow. While the context is in the study of flow and comparing with plastic mould injection, the technique can be applied in numerous other areas such as chemical or biological agent.

In detailing the analytic scheme, the phenomena of distorted circular flow front near the corners (as shown in figure 1(a)) and non-uniform flow front spacing during congestion (as shown in figure 1(b)) need further investigation. Furthermore, the domain discussed in this paper is of Euclidean space, flow front propagation (and hence, the geodesics) in a non-Euclidean space needs more exploration.

References

Au, C. K.; Woo, T. C. (2004): Geometry of inhibition and activation in kinematic waves. **Computer-aided Design**, Vol. 36, No. 12, pp. 1253-1261

Cheng, L-T.; Kang, M.; Osher, S.; Shim, H.; Tsai, Y-H. (2004): Reflection in a Level Set Framework for Geometric Optics, *CMES: Computer Modeling in Engineering & Sciences*, Vol. 5, No. 4, pp. 347-360

Chopp, D. L. (1993): Computing minimal surfaces via level set curvature flow. *Journal of Computational physics.* 106, pp77-91

Defermos, C. M. (1972): Polygonal approximations of solutions of the initial value problem of a conservation law. *Journal of Mathematics and Applications.* Vol 38, pp33-41

Holden, H.; Holden, L.; Hoegh-Krohn, R. (1988): A numerical method for first order non-linear scalar conservation laws in one dimension. *Computational Mathematics Applications.* 15, pp595-602

Okabe, A.; Boots, B.; Sugihara, K.; Chiu, S. N. (2000): Spatial tessellations-concepts and applications of voronoi diagrams. Wiley, Chichester, second edition.

Quadros, W. R.; Ramaswami, K.; Prinz, F. B.; Gurumoorthy, B. (2000): Laytracks: a new approach to automated quadrilateral mesh generation using MAT. Proceedings, 9th International Meshing Roundtable, Sandia National Laboratories, pp.239-250

Sethian, J. A. (1996): A marching level set method for monotonically advancing fronts. *Proceeding of National Academy of Sciences*, 93(4), pp1591-1595

Sethian, J. A. (1999): Level set methods and fast marching methods: evolving interfaces in computational geometry, fluid mechanics, computer vision and materials science. Cambridge University Press.

Sheen, D.; Seo, S.; Cho, J. (2003): A Level Set Approach to Optimal Homogenized Coefficients. *CMES: Computer Modeling in Engineering & Sciences*, Vol. 4, No. 1, pp. 21-30